JOURNAL OF GEOPHYSICAL RESEARCH, VOL. 112, D02308, doi:10.1029/2006JD007450, 2007

Chemical cycling and deposition of atmospheric mercury: Global constraints from observations

Noelle E. Selin,[1,2] Daniel J. Jacob,[1,2] Rokjin J. Park,[1,2] Robert M. Yantosca,[1,2] Sarah Strode,[3] Lyatt Jaeglé,[3] and Daniel Jaffe[4]

Received 27 April 2006; revised 30 June 2006; accepted 9 August 2006; published 30 January 2007.

[1] We use a global 3-D model of atmospheric mercury (GEOS-Chem) to interpret worldwide observations of total gaseous mercury (TGM) and reactive gaseous mercury (RGM) in terms of the constraints they provide on the chemical cycling and deposition of mercury. Our simulation including a global mercury source of 7000 Mg yr^{-1} and a TGM lifetime of 0.8 years reproduces the magnitude and large-scale variability of TGM observations at land sites. However, it cannot capture observations of high TGM from ship cruises, implying a problem either in the measurements or in our fundamental understanding of mercury sources. Observed TGM seasonal variation at northern midlatitudes is consistent with a photochemical oxidation for Hg(0) partly balanced by photochemical reduction of Hg(II). Observations of increasing RGM with altitude imply a long lifetime of Hg(II) in the free troposphere. We find in the model that Hg(II) dominates over Hg(0) in the upper troposphere and stratosphere and that subsidence is the principal source of Hg(II) at remote surface sites. RGM observations at Okinawa Island (Japan) show large diurnal variability implying fast deposition, which we propose is due to RGM uptake by sea-salt aerosols. Observed mercury wet deposition fluxes in the United States show a maximum in the southeast, which we attribute to photochemical oxidation of the global Hg(0) pool. They also show a secondary maximum in the industrial Midwest due to regional emissions that is underestimated in the model, possibly because of excessive dry deposition relative to wet (dry deposition accounts for 68% of total mercury deposition in the United States in the model, but this is sensitive to the assumed phase of Hg(II)). We estimate that North American anthropogenic emissions contribute on average 20% to U.S. mercury deposition.

Citation: Selin, N. E., D. J. Jacob, R. J. Park, R. M. Yantosca, S. Strode, L. Jaeglé, and D. Jaffe (2007), Chemical cycling and deposition of atmospheric mercury: Global constraints from observations, *J. Geophys. Res.*, *112*, D02308, doi:10.1029/2006JD007450.

1. Introduction

[2] Concern over the toxicity and human health risks of mercury deposited to ecosystems and bioaccumulating as methyl mercury in fish has prompted efforts to regulate anthropogenic emissions. Current atmospheric concentrations of mercury are 3 times higher than preindustrial values [*Mason et al.*, 1994]. Effective regulation requires knowledge of source receptor relationships; such knowledge, however, is limited by large uncertainties in mercury sources, atmospheric chemistry, and deposition processes. A critical uncertainty is the redox chemistry between gaseous elemental mercury (Hg(0)), which has an atmospheric lifetime ~1 year, and Hg(II), the principal deposited form [*Mason and Sheu*, 2002; *Pehkonen and Lin*, 1998; *Schroeder and Munthe*, 1998]. Extensive atmospheric measurements have become available in the last few years that can provide constraints on the chemical cycling and deposition of mercury. We use here a global 3D chemical transport model (GEOS-Chem CTM) to interpret these observations from a global budget perspective and to estimate the relative contributions of domestic and international sources to mercury deposition in the United States.

[3] Direct anthropogenic releases of mercury are primarily from coal-fired power plants, metal smelting, and waste incineration [*Pacyna et al.*, 2005; *Streets et al.*, 2005], and contribute about one third of the current emissions to the atmosphere [*Mason and Sheu*, 2002]. Other sources are oceans, soils, terrestrial vegetation, and biomass burning; these sources include both a natural component and an anthropogenic component from recycling of previously deposited mercury [*Mason and Sheu*, 2002]. Recycling

[1]Department of Earth and Planetary Sciences, Harvard University, Cambridge, Massachusetts, USA.
[2]Division of Engineering and Applied Sciences, Harvard University, Cambridge, Massachusetts, USA.
[3]Department of Atmospheric Sciences, University of Washington, Seattle, Washington, USA.
[4]Interdisciplinary Arts and Sciences, University of Washington, Bothell, Washington, USA.

0148-0227/07/2006JD007450$09.00

through the ocean is included in GEOS-Chem with a coupled ocean-atmosphere model [*Strode et al.*, 2006]. Previous global model studies have examined the constraints on the mercury sources from atmospheric observations of total gaseous mercury (TGM) [*Bergan and Rodhe*, 2001; *Ryaboshapko et al.*, 2002; *Seigneur et al.*, 2004]. We focus here on exploiting the spatial and temporal variability in worldwide observations of both TGM and reactive gaseous mercury (RGM, representing the gas-phase component of Hg(II)) as constraints on atmospheric redox and deposition processes.

[4] Much of the limitation in using atmospheric models to quantify source receptor relationships for mercury deposition arises from the uncertainty in mercury redox chemistry. Ozone and OH are generally assumed to be the main global Hg(0) oxidants [*Lin et al.*, 2006], but the mechanisms and rates are poorly understood [*Calvert and Lindberg*, 2005]. Halogen oxidants could also be important [*Holmes et al.*, 2006; *Lin et al.*, 2006], and this is well established in Arctic spring where rapid conversion of Hg(0) to Hg(II) is observed [*Schroeder et al.*, 1998]. Aqueous-phase reduction of Hg(II) has been observed by *Pehkonen and Lin* [1998], but its mechanism and atmospheric relevance are uncertain [*Gårdfeldt and Jonsson*, 2003].

[5] A few previous global model studies have examined the constraints from atmospheric TGM observations on the atmospheric chemistry of mercury. *Bergan and Rodhe* [2001] found that using OH as the only Hg(0) oxidant with the rate constant of *Sommar et al.* [2001], and no Hg(II) reduction, resulted in average Hg(0) concentrations a factor of three below observed values in North America and Europe. *Seigneur et al.* [2004] included gas-phase oxidation of Hg(0) by O_3, OH, and Cl_2, as well as aqueous redox chemistry, resulting in annual average TGM concentrations consistent with observations and an atmospheric lifetime for TGM of 1.2 years. We go beyond these previous model studies by using extensive observations of both TGM and RGM, and by examining the information contained in both the spatial and temporal patterns for constraining the chemistry and deposition of mercury. The data sets include monitoring observations from major networks in Europe (EMEP), Canada (CAMNet), and the United States (MDN) [*Ebinghaus et al.*, 2002; *Kellerhals et al.*, 2003; Co-operative Programme for Monitoring and Evaluation of the Long-Range Transmissions of Air Pollutants in Europe (EMEP), EMEP measurement data, edited, accessed via internet, hereinafter referred to as EMEP, 2005; Environment Canada, 2003, Canadian Atmospheric Mercury Network, Data, Meterological Service of Canada, Toronto, hereinafter referred to as Environment Canada, 2003]. They also include research data sets from surface sites [*Baker et al.*, 2002; *Jaffe et al.*, 2005], ship cruises [*Lamborg et al.*, 1999; *Laurier et al.*, 2003; *Temme et al.*, 2003a], and aircraft [*Banic et al.*, 2003; *Friedli et al.*, 2004]. Anthropogenic emissions in the model are for the year 2000 [*Pacyna et al.*, 2005; *Wilson et al.*, 2005], and we focus our analysis on 1998–2005 observations.

2. Model Description

2.1. General Description

[6] We use the GEOS-Chem CTM version 7.04 (http://www.as.harvard.edu/chemistry/trop/geos/) [*Bey et al.*, 2001] to simulate three species of mercury in the atmosphere: elemental mercury (Hg(0)), divalent mercury (Hg(II)), and primary particulate mercury (Hg(P)). Hg(II) can partition between the gas and particulate phases. Primary Hg(P) is assumed to be nonvolatile and chemically inert, and we deposit it as a submicron aerosol.

[7] Our simulation is conducted for a 6-year period (2000–2005), with the first 3 years used for initialization. It uses assimilated meteorological data from the NASA Goddard Earth Observing System (GEOS-4), including winds, mixed layer depths, temperature, precipitation, and convective mass fluxes. These data are available with 6-hour temporal resolution (3 hours for surface quantities and mixing depths), a horizontal resolution of $1^\circ \times 1.25^\circ$, and 55 hybrid sigma-pressure levels in the vertical. We degrade the horizontal resolution to $4^\circ \times 5^\circ$ for input to GEOS-Chem. We focus most of our analyses on model statistics for 2003, but also use 2004 and 2005 results for comparison to observations taken in those years.

2.2. Mercury Emissions

[8] We use the Global Emission Inventory Activity (GEIA) global inventory of anthropogenic emissions for the year 2000. This inventory includes Hg(0), Hg(II), and Hg(P) at 1278, 720, and 192 Mg yr^{-1}, respectively, with a horizontal resolution of 1° by 1° and no seasonal variation [*Pacyna et al.*, 2005; *Wilson et al.*, 2005]. Major sources in that inventory are electric power generation and waste incineration. Mobile sources are not consistently included, although recent data suggest that they could be significant [*Edgerton and Jansen*, 2004; *Lynam and Keeler*, 2006]. The global emission rate of anthropogenic mercury declined by 5.5% from 1995 to 2000 according to GEIA, but there have been more substantial regional changes. Emissions in the United States and Russia declined by 12% and 46% respectively, while emissions in India, Brazil, Mexico, and Spain increased. Emissions in China declined 1.9%. Asia accounted for 54% of global anthropogenic mercury emissions in 2000.

[9] Oceans and land are major natural sources of Hg(0), involving both primary emission (from ocean upwelling and mercury-containing rocks) and reemission of previously deposited mercury. We use the GEOS-Chem ocean model of *Strode et al.* [2006] dynamically coupled to our atmospheric simulation. This model includes three species of mercury in the oceanic mixed layer: Hg(0), Hg(II), and nonreactive nonvolatile mercury. Hg(0) and Hg(II) exchange with the atmosphere and with the deep ocean but are not transported horizontally. In the oceanic mixed layer, Hg(II) is converted to Hg(0) and to nonreactive mercury at rates proportional to the local net primary productivity. These rates are adjusted by *Strode et al.* [2006] to match mean oceanic observations of elemental, reactive, and total aqueous mercury. The resulting Hg(0) net emission from the ocean is 2800 Mg yr^{-1}.

[10] We include a primary land source of 500 Mg yr^{-1} [*Lindqvist*, 1991] distributed following the locations of mercury mines [*Frank*, 1999] as an indicator of mercury deposits. Land emissions are known to vary with temperature, solar radiation, and precipitation [*Gustin et al.*, 1997] but we ignore this variability here due to lack of quantitative information. We map reemission of mercury previously

deposited to land according to the deposition patterns of current sources, following the methodology of *Bergan et al.* [1999] and *Seigneur et al.* [2001]. This is consistent with *Schlüter* [2000], who argues that most of upper soil mercury outside of areas with large natural mercury deposits originates from atmospheric mercury deposition. We scale the total global reemission to 1500 Mg yr^{-1}, at the low end of the range estimated by *Lindberg et al.* [1998], and more consistent with other literature [*Mason and Sheu*, 2002]. We neglect the uncertain contributions of emissions from volcanoes and biomass burning, the former estimated between 110 and 700 Mg yr^{-1} [*Nriagu and Becker*, 2003; *Pyle and Mather*, 2003], and the latter between 100 and 860 Mg yr^{-1} [*Friedli et al.*, 2001].

2.3. Mercury Chemistry

[11] The model includes Hg(0) oxidation to Hg(II) by OH ($k = 9 \times 10^{-14}$ cm^3 s^{-1} [*Pal and Ariya*, 2004a; *Sommar et al.*, 2001]) and ozone ($k = 3 \times 10^{-20}$ cm^3 s^{-1} [*Hall*, 1995]). No temperature dependence is included in these rate constants due to lack of data. Oxidation rates are calculated using archived monthly mean 3-D fields of OH and O_3 concentrations from a detailed GEOS-Chem tropospheric chemistry simulation [*Park et al.*, 2004]. We distribute the OH concentration during daytime hours as the cosine of the solar zenith angle. The resulting lifetime of Hg(0) is 0.31 years against oxidation, with OH providing the dominant sink (83%). *Pal and Ariya* [2004b] reported $k = 7.5 \times 10^{-19}$ cm^3 s^{-1} for Hg(0) oxidation by ozone, but this would imply an Hg(0) atmospheric lifetime of ~20 days which is inconsistent with observations as discussed below.

[12] The chemical speciation of Hg(II) measured in the atmosphere as RGM is unknown [*Mason and Sheu*, 2002]; the Hg(II) product of the reactions of Hg(0) with O_3 and OH is likely HgO [*Sommar et al.*, 2001]. HgO is very soluble in water (Henry's Law constant of 2.7×10^{12} M atm^{-1}), and thus dissolves in aqueous aerosols and clouds [*Schroeder and Munthe*, 1998]. In the aqueous phase, HgO dissociates to Hg^{2+} [*Pleijel and Munthe*, 1995]. Under most atmospheric conditions, Cl^- concentrations in the aqueous phase are sufficiently high to drive recomplexation to $HgCl_2$ [*Lin and Pehkonen*, 1998], which has a Henry's Law constant of 1.4×10^6 M atm^{-1} [*Lin and Pehkonen*, 1999] and should thus volatilize from the aqueous aerosol except in the presence of cloud. Following *Lin et al.* [2006], we view Hg(II) as $HgCl_2$ for purpose of calculating gas-aqueous partitioning relevant to in-cloud reduction and wet and dry deposition.

[13] Aqueous-phase photochemical reduction of Hg(II) to Hg(0) has been observed in the laboratory and in irradiated rainwater samples [*Pehkonen and Lin*, 1998; J. Lin, personal communication, 2003] but it remains uncertain and the mechanism is unknown [*Gårdfeldt and Jonsson*, 2003; *Goodsite et al.*, 2004]. We include it in our model as an in-cloud photochemical process applied to dissolved Hg(II) and scaled to match constraints on TGM lifetime and seasonal variation as described below. Dissolved Hg(II) is obtained from the cloud fraction in each gridbox diagnosed by the gridbox relative humidity [*Sundqvist et al.*, 1989] and the corresponding in-cloud liquid water content diagnosed by the gridbox temperature [*Somerville and Remer*, 1984]. The photoreduction rate constant (s^{-1}) applied to aqueous Hg(II) is parameterized as 8.4×10^{-10} [OH], where [OH] is the gas-phase concentration in units of molecules cm^{-3} also used to compute Hg(0) oxidation. This rate constant results in a mean lifetime of 20 min for dissolved Hg(II) in cloud in the model. The in-cloud reduction scheme is applied in the model over 30-min time steps as part of the overall mercury chemistry module, and the corresponding Hg(II) reduction rate is thus principally determined by this length of the time step; we effectively assume that air resides for 30 minutes in cloud.

2.4. Mercury Deposition

[14] Wet deposition of mercury in GEOS-Chem is applied to Hg(II) and Hg(P), but not to Hg(0) because of its low Henry's Law constant (0.11 M atm^{-1} at 298K [*Lin and Pehkonen*, 1999]). The simulation of wet deposition includes rainout and washout from large-scale and convective precipitation, and scavenging in convective updrafts [*Liu et al.*, 2001]. We assume that Hg(II) is scavenged quantitatively by liquid precipitation but is released to the gas phase when water freezes (zero retention efficiency). Hg(P) is scavenged with the same efficiency as a water-soluble aerosol [*Liu et al.*, 2001].

[15] Dry deposition of Hg(0) to the ocean in GEOS-Chem is simulated as part of the bidirectional exchange model of *Strode et al.* [2006] presented above. Dry deposition of Hg(0) to land is neglected, although there is some evidence of bidirectional exchange [*Lindberg et al.*, 1998; *Poissant et al.*, 2004a]. Dry deposition of Hg(II) and Hg(P) is simulated with a standard resistance-in-series scheme based on local surface type and turbulence [*Wang et al.*, 1998; *Wesely*, 1989]. We assume zero surface resistance for Hg(II), consistent with observations of very high deposition velocities including 7.6 cm s^{-1} as a median value over wetlands in summer [*Poissant et al.*, 2004b] and 5–6 cm s^{-1} in the daytime over a forest in summer [*Lindberg and Stratton*, 1998]. Simulated monthly mean dry deposition velocities exceed 3 cm s^{-1} over land in summer.

[16] We also include in GEOS-Chem a uniform first-order sink for Hg(II) throughout the marine boundary layer (MBL) to simulate uptake by sea-salt aerosols followed by deposition. Coastal measurements in Florida show evidence of this uptake [*Malcolm et al.*, 2003], and it represents our best explanation for the low concentrations and large diurnal variation of RGM observed at Okinawa Island by *Jaffe et al.* [2005], as discussed below. We assume a time constant of 7 h for uptake of Hg(II) by sea salt uniformly throughout the MBL, which we set to match the Okinawa constraints. This time constant is consistent with expected uptake rates for soluble gases; a GEOS-Chem simulation by *Alexander et al.* [2005] derived a mean uptake time constant of 1 h for HNO_3 by sea salt in the MBL.

2.5. Global Mercury Budget

[17] Figure 1 shows the global budget of mercury in GEOS-Chem, including the cycling between different components. Hg(0) has a lifetime against oxidation of 4 months, but reduction of Hg(II) brings the overall lifetime of TGM up to 0.79 years (9.5 months). Hg(II) has a tropospheric lifetime of 16 days against deposition; this relatively long lifetime for a soluble gas is due to a dominant contribution of higher altitudes to the inventory, as discussed below.

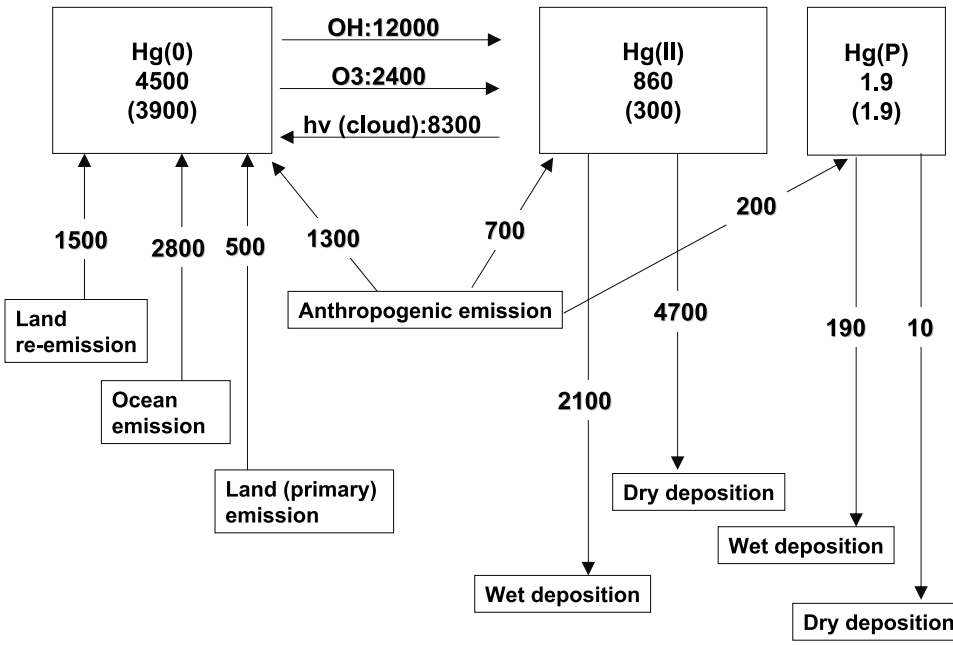

Figure 1. Global atmospheric mercury budget in GEOS-Chem. Inventories are in Mg and rates are in Mg yr^{-1}. Tropospheric inventories are given in parentheses (most of atmospheric Hg(II) is in the stratosphere).

[18] Table 1 compares the GEOS-Chem TGM budget to those from previous global model studies. Literature values for the TGM lifetime average 1.1 ± 0.3 years, reflecting observational constraints in particular from the interhemispheric gradient [*Bergan et al.*, 1999; *Lamborg et al.*, 2002; *Mason et al.*, 1994; *Mason and Sheu*, 2002; *Seigneur et al.*, 2004; *Seigneur et al.*, 2001; *Shia et al.*, 1999], although we will argue below that these constraints are more consistent with a shorter lifetime. Dry deposition in GEOS-Chem dominates globally over wet deposition. The RGM sink via uptake onto sea-salt aerosols contributes 33% to global dry deposition. The sources and sinks in Table 1 carry much larger uncertainties than is apparent from the range of global model budgets, since different models tend to follow similar parameterizations and assumptions for emissions and chemistry.

3. Annual Mean Concentrations of TGM and Interhemispheric Gradient

[19] Figure 2 (top panel) shows observed annual mean concentrations of TGM in surface air compared to model results. TGM in the model is taken as the sum of Hg(0) and Hg(II); this ignores the partitioning of Hg(II) into the aerosol but the associated error is small since Hg(0) is the dominant component of surface TGM. The measurements include 1998–2004 annual mean data from 22 nonurban land-based sites, 20 in the northern hemisphere and two in

Table 1. Global Present-Day Budgets of Total Gaseous Mercury (TGM) in the Literature

	Mason et al. [1994]	*Bergan et al.* [1999]	*Shia et al.* [1999]	*Seigneur et al.* [2001]	*Lamborg et al.* [2002]	*Mason and Sheu* [2002]	*Seigneur et al.* [2004][a]	This Work
Total sources (Mg yr^{-1})[b]	7000	6050	6100	6107	4400	6600	6410	7000
Primary anthropogenic	4000	2150	2100	2104	2600	2400	2140	2200
Primary land	1000	500	2000	500	1000	810	630	500
Reemission land	1000	2000	2000	1500	1000	790	1670	1500
Primary ocean	2000	1400	2000	2000	800	1300	442	400
Reemission ocean	2000	1400	2000	2000	800	1300	1536	2400
Total sinks (Mg yr^{-1})	7000	6050[c]	6100	6107[d]	4200	6600	6410	7000
Wet deposition			2800			3920		2100
Dry deposition			3300			2680		4700[e]
TGM burden	5000	6050	10400	6900[e]	5220	5000	7690[e]	5360
TGM lifetime (y)	0.71[f]	1.0	1.7	1.1	1.3	0.76	1.2	0.79[g]

[a]Base case scenario.
[b]We distinguish between "primary" emissions that originate from outside the Earth surface reservoirs (atmosphere, soil, vegetation, ocean mixed layer) and "re-emissions" that involve recycling between the surface reservoirs.
[c]Not given; assumed here from steady state; dry deposition is stated as contributing less than 15% to total deposition.
[d]Not given; assumed here from steady state.
[e]Including 1540 Mg y^{-1} from uptake by sea-salt aerosols followed by deposition.
[f]Mason et al. quote a lifetime of 1 year, which excludes 2000 Mg y^{-1} anthropogenic emissions deposited near source regions.
[g]TGM lifetime versus deposition of Hg(II). There is also a sink from oceanic uptake of Hg(0) although the ocean is a net source [*Strode et al.*, 2006].

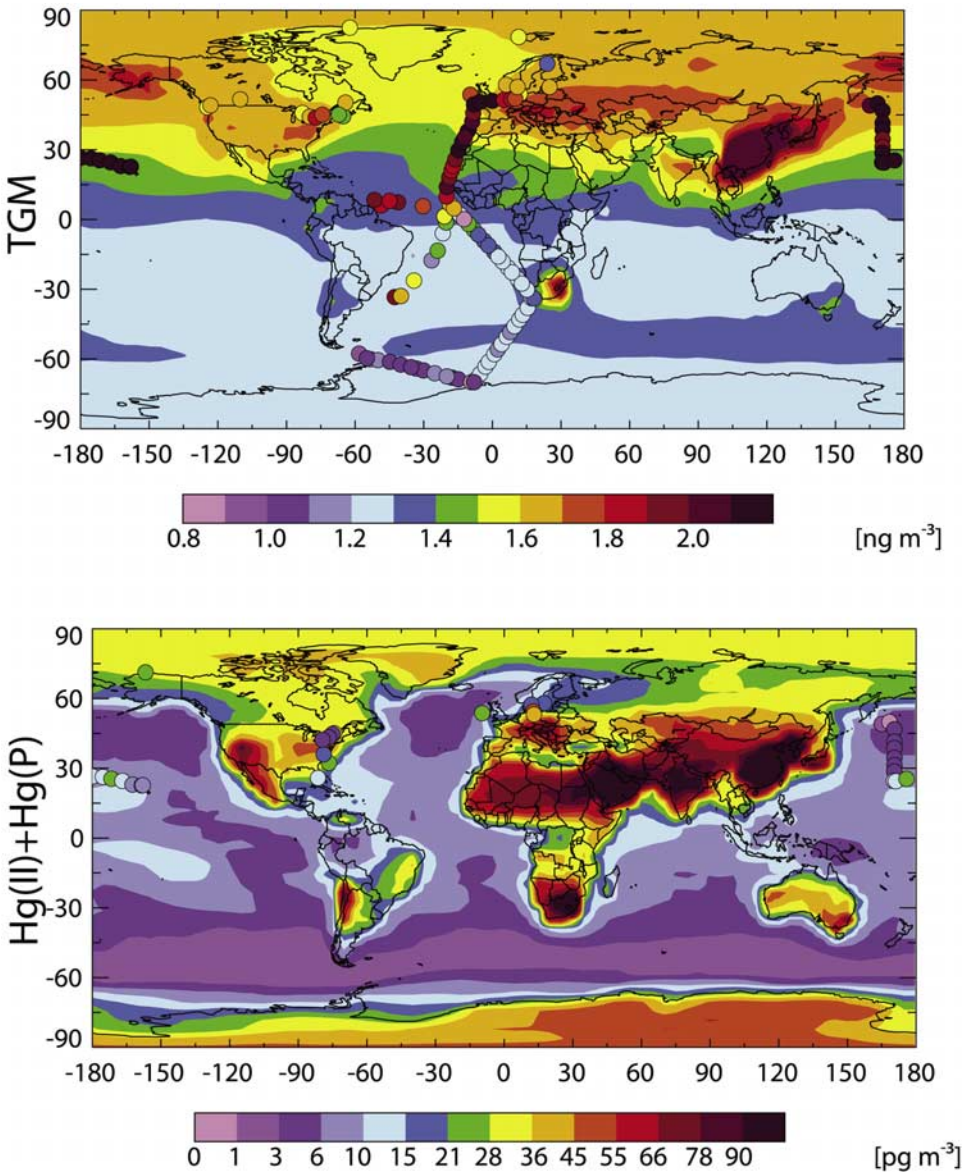

Figure 2. Annual average mercury concentrations in surface air. Model results (background, for year 2003) are compared to observations (circles) from long-term surface sites (Tables 2 and 3). Also shown are observations from ship cruises in the tropical Atlantic in May–June 1996 [*Lamborg et al.*, 1999], across the Atlantic (north-south transect) in December 1999 to January 2000 from *Temme et al.* [2003b], and across the NW Pacific in May–June 2002 from *Laurier et al.* [2003]. The top panel shows total gaseous mercury (TGM) in the observations, and the sum of Hg(0) and Hg(II) in the model. The bottom panel shows the sum of reactive gaseous mercury (RGM) and total particulate mercury (TPM) in the observations, and the sum of Hg(II) and Hg(P) in the model. TPM observations are not available for some sites in Table 3 and for the *Laurier et al.* [2003] cruise, and in those cases we plot RGM observations only. Color scales are saturated at the maximum values indicated in the legend.

the southern hemisphere (Table 2). Model results are for 2003, with anthropogenic emissions for 2000. We also show in Figure 2 observations from three ship cruises although these do not represent annual means (see caption).

[20] The mean annual TGM concentration observed at all 22 land-based sites in Table 2 is 1.58 ± 0.19 ng m^{-3}, and this is reproduced by the model with no mean bias (1.63 ± 0.10 ng m^{-3}). GEOS-Chem agrees within 0.10 ng m^{-3} at 12 sites, and the model can account for 51% of the spatial variance in the measurements (r^2 = 0.51). GEOS-Chem overestimates concentrations at the two southern hemisphere sites of Cape Point, South Africa and Neumayer Station, Antarctica. Cape Point in the model is affected by a large industrial source in South Africa (Figure 2).

[21] The cruise data in the northern hemisphere show systematically higher concentrations than the land-based sites at corresponding latitudes (Figure 3). The model shows the opposite pattern, reflecting its dominant continental

Table 2. Long-Term Total Gaseous Mercury Measurements Used for Model Evaluation

Site[a]	Observation Years	Annual Mean Concentration, ng m^{-3}		Reference[b]
		Observations	Model (2003)	
Alert, Canada (82N, 62W)*	1995–2002	1.55	1.57	[1]
Zeppelin, Norway (79N, 12E)*	2000–2004	1.55	1.61	[2]
Pallas, Finland (67N, 24E)*	1998–2002	1.34	1.65	[2]
Lista, Norway (58N, 6E)*	2000–2003	1.68	1.63	[2]
Råö, Sweden (57N, 11E)*	2001	1.66	1.67	[2]
Rörvik, Sweden (57N, 25E)*	2001–2002	1.66	1.70	[2]
Zingst, Germany (54N, 12E)*	2000	1.56	1.74	[2]
Mace Head, Ireland(54N, 10W)*	1995–2001	1.75	1.56	[3]
Langenbrügge, Germany (52N, 10E)*	2002	1.70	1.74	[2]
Esther, Canada (52N, 110W)	1997–1999	1.69	1.63	[4]
Mingan, Canada (50N, 64W)	1997–1999	1.62	1.60	[4]
Delta, Canada (49N, 123W)*	1999–2001	1.73	1.71	[1]
Reifel Island, Canada (49N, 123W)	1997–1999	1.69	1.71	[4]
Cheeka Peak, Washington, United States (48N, 125W)*	2001–2002	1.56	1.71	[5][c]
Burnt Island, Canada (46N, 83W)	1997–1999	1.58	1.66	[4]
St. Anicet, Canada (45N, 74W)*	1997–1999, 2001	1.70	1.65	[4], [6]
St. Andrew, Canada (45N, 67W)*	1997–1999, 2001	1.41	1.60	[1]
Kejimkujik, Canada (44N, 65W)*	2001	1.49	1.60	[1]
Egbert, Canada (44N, 80W)	1997–1999	1.65	1.67	[4]
Pt. Petre, Canada (44N, 77W)	1997–1999	1.90	1.70	[4]
Cape Point, South Africa (34S, 19E)	1998–2002	1.23	1.54	[7]
Neumayer, Antarctica (70S, 8W)	2000	1.06	1.26	[8]

[a]Asterisk indicates that monthly mean observations are also available from the reference; the monthly data are used in Figure 4.
[b](1) Environment Canada (2003); (2) EMEP (2005); (3) *Ebinghaus et al.* [2002]; (4) *Kellerhals et al.* [2003]; (5) *Weiss-Penzias et al.* [2003]; (6) *Poissant et al.* [2005]; (7) *Baker et al.* [2002]; (8) *Ebinghaus et al.* [2002].
[c]Hg(0) data.

source of mercury and consistent with the patterns found in previous global models [*Seigneur et al.*, 2004]. The model is thus biased low relative to the cruise data in the northern hemisphere. The *Temme et al.* [2003b] cruise data extending from high northern to high southern latitudes show a considerably stronger interhemispheric gradient than is found in the land-based data or in the model. Though we might not expect to capture episodic mercury-rich plumes transported to sea in our model, we underestimate the cruise data throughout the northern hemisphere. *Strode et al.* [2006] show that increasing ocean emissions results in better agreement with northern hemisphere cruise data but overestimates southern hemisphere data. An increase of natural land sources in northern Africa could also contribute to higher levels over the North Atlantic.

[22] Several previous studies have used observations of the TGM interhemispheric gradient to place constraints on the atmospheric lifetime of mercury, although confidence in the approach would require reconciliation of the apparent inconsistency between the land-based and cruise data. *Lamborg et al.* [2002] estimated the range of plausible interhemispheric TGM concentration ratios for surface air as between 1.2 and 1.8. *Temme et al.* [2003b] reported an average interhemispheric ratio of 1.49 ± 0.12 from several Atlantic cruises in 1996–2001, and inferred from this a 1-year atmospheric lifetime for TGM. In GEOS-Chem the zonal mean interhemispheric ratio at the surface is 1.2, and the corresponding TGM lifetime is 0.79 years; this ratio is consistent with the land-based data (Figure 3) but lower than the cruise data. Increasing the ratio in the model would require a shorter TGM lifetime, but as discussed below this would compromise simulation of the seasonal variation in TGM concentrations at surface sites. A change in the ratio of emissions between the northern and southern hemisphere, as discussed above in the interpretation of the northern hemisphere cruise data, could also alter the interhemispheric concentration ratio.

4. TGM Seasonal Variation

[23] Figure 4 shows the simulated versus measured seasonal variations of TGM concentrations at the two Arctic sites and 12 northern midlatitudes sites of Table 2 for which monthly resolved data are available. The Arctic observations show the well-known minimum in spring due to Hg(0) oxidation by halogen radicals followed by Hg(II) deposition [*Schroeder et al.*, 1998]. This halogen chemistry is not included in the model, resulting in the seasonal overesti-

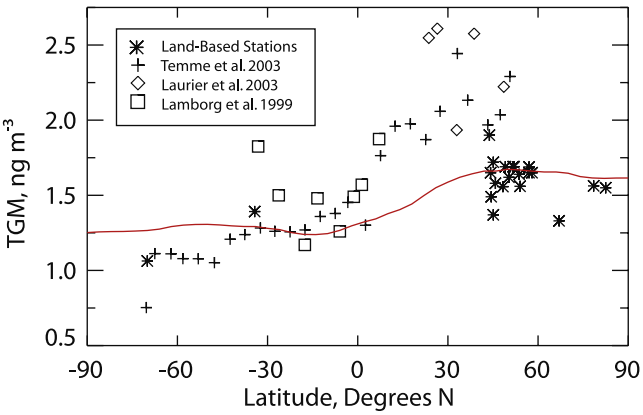

Figure 3. Variation of TGM surface air concentrations with latitude. Zonally averaged, annual mean model results (line) are compared to observations (symbols). The cruise data are those of Figure 2 and are averaged over 4° latitudinal bins; land-based stations are annual means from Table 2.

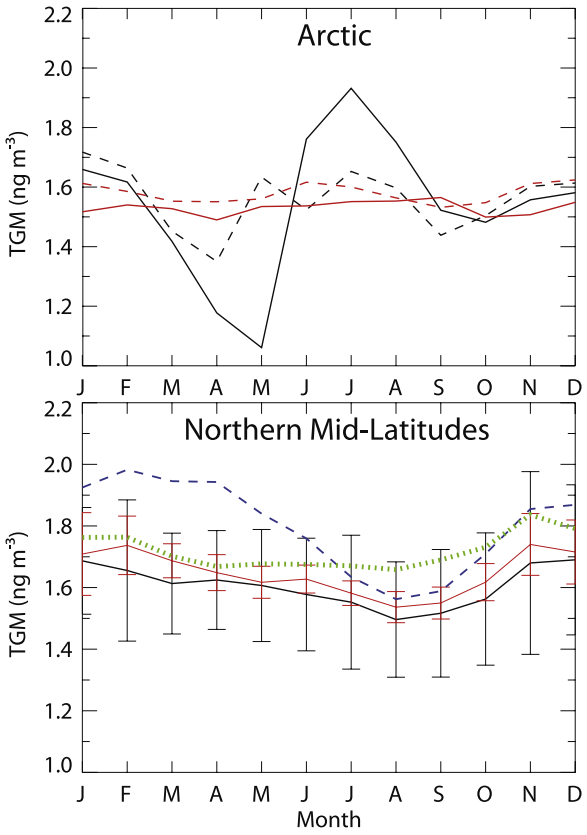

Figure 4. Mean seasonal variation of TGM at the Arctic and northern midlatitudes sites of Table 2. Standard model results (red) are compared to observations (black). The Arctic panel shows data for Alert (solid) and Zeppelin (dashed). The northern midlatitudes panel shows averages for the 12 sites in Table 2 with monthly data available; vertical bars show the standard deviations of the monthly means across sites. Blue dashed and green dotted lines show results from sensitivity simulations with OH and O_3 as the only Hg(0) oxidants, respectively (see text).

mate. The Hg(0) depletion in the observations is confined to below 1 km altitude, as shown by aircraft profiles taken in springtime over Arctic Canada [*Banic et al.*, 2003]. Much of the depleted mercury is reemitted from the snowpack in summer [*Steffen et al.*, 2005], as reflected by the observed summer maximum in Figure 4 that largely balances the spring depletion.

[24] Measurements of TGM at most northern midlatitudes sites in Table 2 show a seasonal trend with high concentrations in winter and spring, and low concentrations in summer and fall [*Kellerhals et al.*, 2003; Environment Canada, 2003]. Two of the sites in Table 2, Cheeka Peak (Washington) and Lista (Norway) show an opposite seasonal variation for reasons that are unclear [*Weiss-Penzias et al.*, 2003]. For the ensemble of 12 northern midlatitudes sites in Table 2 with available monthly data, the mean difference between the seasonal maximum (January) and minimum (August) is 0.19 ng m^{-3} and statistically significant ($p < 0.02$). The model closely reproduces this seasonal variation, with a seasonal amplitude from minimum to maximum of 0.17 ng m^{-3}. The model seasonal variation would be stronger if the dominant photochemical oxidation of Hg(0) in the model (Figure 1) were not partly compensated by photoreduction of Hg(II). This is illustrated in Figure 4 by results from sensitivity simulations with either OH or O_3 as only Hg(0) oxidant, no photochemical reduction, and oxidation rate constants adjusted to maintain a TGM lifetime of 0.79 years. The OH-only simulation shows a seasonal amplitude (0.36 ng m^{-3}) much higher than observed, while the O_3-only simulation underestimates the seasonal amplitude (0.10 ng m^{-3}) and has a poorly defined seasonal phase. An uncertainty in this analysis is that we do not take into account seasonal variation in the reemission of mercury from land, which would tend to dampen the seasonal amplitude in the TGM observations. We also do not take into account the temperature dependence of Hg(0)/Hg(II) redox kinetics due to lack of information, and this could also affect the simulation of the seasonal amplitude.

5. Vertical Profiles of Hg(0)

[25] Aircraft vertical profiles of Hg(0) mixing ratios up to 7 km altitude have been reported by *Banic et al.* [2003] over Ontario in winter and by *Friedli et al.* [2004] near southern Japan in spring. *Banic et al.* [2003] find no significant vertical trend (±10%); the corresponding model fields for the same region and season show a 10% monotonic decline from 0 to 7 km. Comparison of model results to the *Friedli et al.* [2004] data is shown in Figure 5. The observations show two maxima, in the boundary layer and at 5–7 km altitude. The model reproduces the strong boundary layer enhancement driven by Chinese outflow. However, it shows a monotonic decrease with altitude, reflecting the loss from Hg(0) oxidation, and does not reproduce the observed 5–7 km enhancement. *Friedli et al.* [2004] find that the 5–7 km enhancement is not associated with elevated CO, which argues against a simple pollution influence.

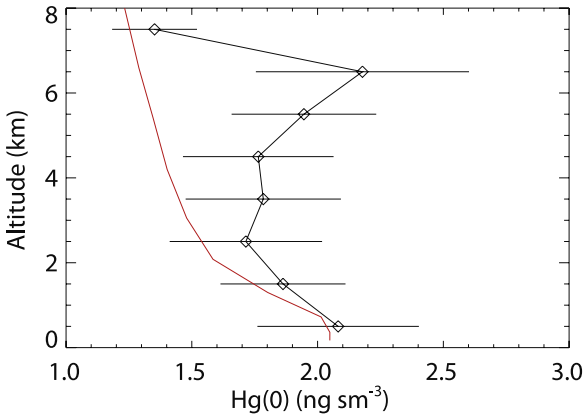

Figure 5. Vertical distribution of Hg(0) mixing ratios near southern Japan. Observations from the ACE-Asia aircraft campaign in April–May 2001 [*Friedli et al.*, 2004] (in black) are compared to monthly mean model results for April over the same domain (in red). The observations are averaged in 1 km bins, and error bars indicate 1 standard deviation. "sm^3" refers to a cubic meter under standard conditions of temperature and pressure, so that "ng sm^{-3}" is a mixing ratio unit.

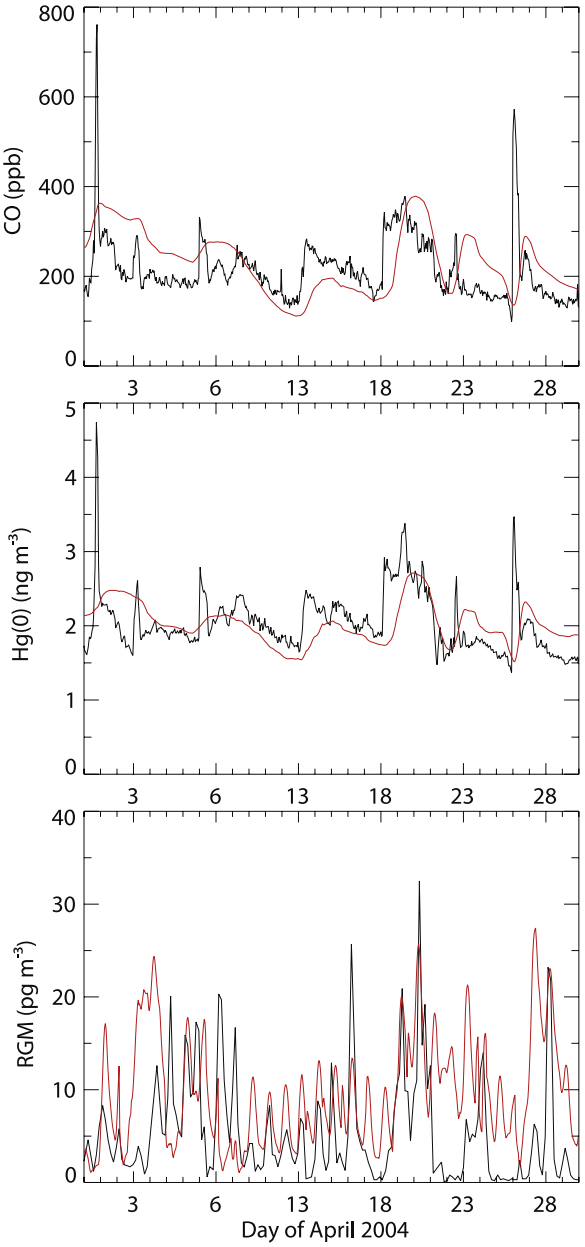

Figure 6. Hg(0), RGM, and CO concentrations at Okinawa in April 2004, Model results (red) are compared to observations from *Jaffe et al.* [2005] (black).

High-altitude recycling of Hg(II) by photolysis might offer an alternate explanation; many Hg(II) complexes including with OH^-, Cl^-, and organic ligands absorb UV radiation [*Nriagu*, 1994]. However, this explanation runs counter to independent evidence for rapid increase of RGM with altitude, as discussed below. In the model, photoreduction of Hg(II) takes place only in the aqueous phase in clouds and is therefore mostly confined to the lower troposphere.

6. Time Series of Hg(0), RGM, and CO at Okinawa

[26] *Jaffe et al.* [2005] report speciated mercury measurements in Asian outflow at Okinawa, Japan (27N, 128E) during April 2004 with near-continuous 3-hour temporal resolution. Figure 6 shows the simulated versus measured time series for CO, Hg(0), and RGM concentrations. The GEOS-Chem CO simulation is as described by *Heald et al.* [2003]. GEOS-Chem reproduces the day-to-day variation in Hg(0) and CO driven by Asian outflow; the slight time offset is due to Okinawa's position at the western edge of the GEOS-Chem (4° × 5°) grid square. The variability of Hg(0) is predominantly driven by Chinese outflow and correlates with CO [*Jaffe et al.*, 2005]. The correlation (r^2) between simulated CO and Hg(0) at Okinawa is 0.91 in the model, compared to 0.84 in measurements. The Hg/CO enhancement ratio determined from the slope of the reduced major axis regression line is 0.0057 ng m^{-3} $ppbv^{-1}$ in the observations as compared to 0.0039 in the model, suggesting that the Asian source of Hg(0) in the model is 30% too low (the CO simulation is unbiased, as shown by *Heald et al.* [2003]). *Jaffe et al.* [2005] previously used their observed Hg(0)/CO enhancement ratio to argue that Asian Hg(0) sources could be as high as 1460 Mg yr^{-1}, as compared with 590 Mg yr^{-1} as Hg(0) in the GEIA 2000 inventory of *Pacyna et al.* [2005] (that inventory includes in addition 460 Mg yr^{-1} anthropogenic mercury from Asia emitted as RGM and Hg(P)). The total Asian source of Hg(0) in GEOS-Chem is 1180 Mg yr^{-1}, including emission from land added to the GEIA 2000 inventory.

[27] Total particulate mercury (TPM) observed by *Jaffe et al.* [2005] at Okinawa correlates weakly with Hg(0) and CO (r^2 = 0.24 and 0.25, respectively), and does not correlate with RGM. Mean observed TPM is 3.0 pg m^{-3}, compared to 12 pg m^{-3} Hg(P) in the model, suggesting that the GEIA inventory overestimates particulate emissions of mercury.

[28] RGM at Okinawa does not correlate significantly with CO or Hg(0), either in the model or in the observations (Figure 6). Observed multiday periods of elevated RGM are generally captured by the model, where they reflect low wind speeds suppressing RGM deposition. The observations show a large diurnal cycle, which we display in Figure 7 as the residual diurnal variation after removal of the 24-hour running mean from the data shown in Figure 6. There is a peak in RGM at 13 local time (LT) and a broad minimum at night. Such a midday RGM maximum has been observed previously in the marine boundary layer [*Hedgecock et al.*, 2003; *Lindberg and Stratton*, 1998] and over land [*Poissant et al.*, 2005]. It implies a photochemical source of RGM and a fast nonphotochemical sink, presumably from deposition. We find in GEOS-Chem that deposition of gas-phase Hg(II) to the ocean (even with zero surface resistance) is not fast enough to drive the midday maximum of RGM. We reproduce it instead by incorporating RGM uptake onto sea-salt aerosol; there is still a 2-hour phase lag in the model diurnal maximum (15 LT). Results from a sensitivity simulation without RGM uptake by sea-salt aerosol show overall RGM concentrations that are 3 times higher than observed, a maximum later in the day at 18 LT, and too slow a decrease at night.

[29] *Hedgecock et al.* [2003] previously observed a similar diurnal variation of RGM in a Mediterranean cruise, but found in a box model simulation that oxidation of Hg(0) by OH could explain only half of the diurnal amplitude. They suggest that oxidation of Hg(0) in the marine boundary layer (MBL) could be driven by the halogen radicals Br and

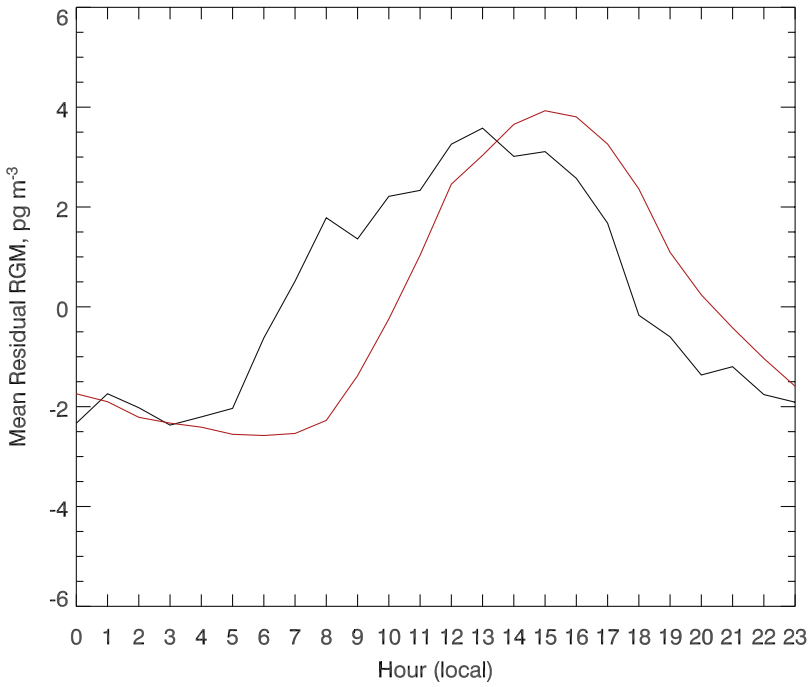

Figure 7. Diurnal variation of RGM concentrations at Okinawa in April 2004, shown as average hourly values after removal of the 24-hour running mean from the data in Figure 6. Model results for Hg(II) (red) are compared to observations from *Jaffe et al.* [2005] (black).

BrO [*Hedgecock and Pirrone*, 2004]. In our simulation, most of the observed diurnal amplitude in RGM at Okinawa can in fact be accounted for on the basis of Hg(0) oxidation by OH. However, the RGM observations show a much steeper increase at sunrise than is simulated by the model (Figure 7), which could indicate Hg(0) oxidation by Br produced from photolysis of Br_2 accumulated at night [*Goodsite et al.*, 2004]. A difficulty with invoking the oxidation of Hg(0) by Br instead of OH would be an increased inconsistency between land-based and ship TGM measurements (section 3), since Br is expected to be higher in the MBL than over land.

7. Global Distribution of Oxidized Mercury

[30] Evaluation of model results for Hg(II) suffers from the ambiguity that Hg(II) in the observations may be partitioned between the gas and aerosol, i.e., between RGM and TPM, while observed TPM also includes the refractory component simulated in the model as Hg(P). RGM/TPM ratios in the observations cover a wide range (Table 3). There is presently

Table 3. Long-term RGM and TPM Measurements Used for Model Evaluation

		Annual Mean Concentrations (pg m^{-3})				
		Observations		Model (2003)		
Site	Observation Years	RGM	TPM	Hg(II)	Hg(P)[a]	Reference[b]
Barrow, Alaska, United States (71N, 157W)	1999–2001[c]	24	NA	23	0.2	[1]
Avspreten, Sweden (58N, 17E)	1998–1999[d]	8	9	18	6	[2][e]
Rörvik, Sweden (57N, 12E)	1998–1999[c]	15	5	18	8	[2][e]
Zingst, Germany (54N, 13E)	1998–1999[c]	25	22	18	13	[2][e]
Mace Head, Ireland (54N, 10W)	1998–1999[c]	18	5	19	2	[2][e]
Neuglobsow, Germany (53N, 13E)	1998–1999[c]	18	25	18	13	[2][e]
St. Anicet, Canada (45N, 74W)	2003	3	26	21	5	[3]
Potsdam, New York, United States (45N, 75W)	2002–2003	4.2	NA	21	5	[4]
Sterling, New York, United States (43N, 77W)	2002–2003	6	NA	21	13	[4]
Stockton, New York, United States (42N, 80W)	2002–2003	5.7	NA	21	15	[4]
Durham, North Carolina, United States (36N, 79W)	1999–2001[f]	16	NA	21	10	[1]
Baltimore, Maryland, United States (32N, 77W)	1999–2001[e]	23	NA	21	4	[1]
Everglades, Florida, United States (26N, 81W)	1999–2001[e]	15	NA	22	2	[1]

[a]GEOS-Chem Hg(P) represents primary-emitted particulate mercury.
[b](1) *Landis et al.* [2002]; (2) *Munthe et al.* [2003]; (3) *Poissant et al.* [2005]; (4) *Han et al.* [2005].
[c]Six field studies between April 1999 and February 2001.
[d]Five campaigns of 14-day duration between November 1998 and November 1999.
[e]Estimated from figure.
[f]Six field studies between April 1999 and February 2001.

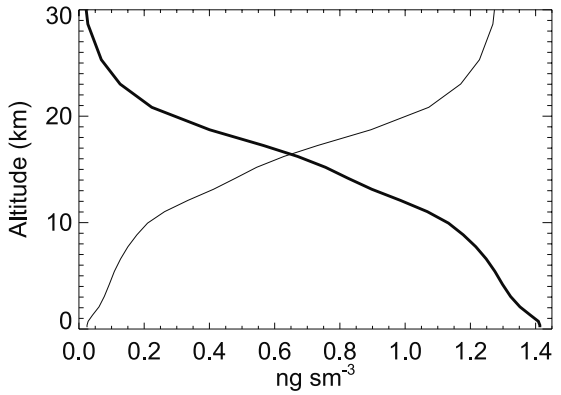

Figure 8. Global annual mean vertical profiles of Hg(0) (bold) and Hg(II) mixing ratios (thin) simulated by the model. "sm^3" refers to a cubic meter under standard conditions of temperature and pressure, so that "ng sm^{-3}" is a mixing ratio unit.

no knowledge of the gas-aerosol partitioning of Hg(II) or of the partitioning of TPM between labile and refractory mercury. We choose to compare in Figure 2 the simulated and observed surface air concentrations of total oxidized mercury, defined as the sum of RGM + TPM in the observations vs. Hg(II) + Hg(P) in the model. TPM data are not always available (Table 3), in which case we still include the corresponding RGM observations in Figure 2.

[31] Continental sites for which RGM+TPM measurements are available observe average concentrations in the range 17–47 pg m^{-3}, while simulated concentrations at the same sites are in the range 21–31 pg m^{-3} (Figure 2 and Table 3). Maximum values are near sources in Germany in both model and measurements. Levels greater than 20 pg m^{-3} are also simulated in polar regions where photochemical reduction is suppressed. Low values over the oceans in the model are due to the sea-salt sink and are consistent with the measurements at Okinawa (see discussion above) and the NW Pacific cruise of *Laurier et al.* [2003]. *Laurier et al.* [2003] show highest values over the central Pacific, which the model reproduces and attributes to low winds, suppressing dry deposition.

[32] In addition to anthropogenic source regions, the model predicts high surface Hg(II) concentrations over elevated land, and over continental deserts where deep vertical mixing brings high-altitude air to the surface (Figure 2). Hg(II) concentrations in the model increase rapidly with altitude because of the sustained source from Hg(0) oxidation and the decrease in efficacy of the Hg(II) sinks from deposition and in-cloud photoreduction. Remarkably, Hg(II) in the model dominates over Hg(0) in the stratosphere (Figure 8). *Sillman et al.* [2005] present measurements from an aircraft campaign off the coast of Florida in June 2000 where RGM concentrations increased from less than 20 pg m^{-3} at the surface to a mean of about 100 pg m^{-3} at 3 km altitude with isolated measurements >200 pg m^{-3}. Their simulation of these observations with the CMAQ regional model shows an increase with altitude from 10 pg m^{-3} at the surface to 40 pg m^{-3} at 3 km but then a slight decrease up to 6 km. The aircraft observations show anticorrelation between Hg(0) and RGM, which is reproduced by CMAQ, but also an anticorrelation between RGM and TGM which is not. Single-particle aircraft measurements by *Murphy et al.* [2006] suggest that most mercury in the lower stratosphere is present in the aerosol phase, and that this mercury originates from oxidation rather than condensation of Hg(0) as the peak is not coincident with the altitude of lowest temperature. This is consistent with our results, assuming that Hg(II) is partitioned into the aerosol at the cold temperatures of the lower stratosphere. Although Figure 8 shows relatively smooth vertical gradients of Hg(0) and Hg(II) from the troposphere to the stratosphere in a global mean sense, we would expect in the observations to find sharp gradients at the local tropopause.

[33] Further evidence for increasing Hg(II) concentrations with altitude is offered by data from mountaintop sites. Measurements at Mauna Loa Observatory, Hawaii (4 km altitude) show RGM levels higher than sea level measurements [*Renner*, 2004]. May–August 2005 measurements made by *Swartzendruber et al.* [2006] at Mt. Bachelor, Oregon (2.7 km a.s.l.) show a mean of 43 pg $m^{-3}$and significant negative correlation with water vapor. Taking into account only RGM nighttime data greater than 50 pg m^{-3} over 6-hour periods, *Swartzendruber et al.* find in their observations a strong negative correlation between RGM and Hg(0) ($r^2 = 0.80$) with regression slope dRGM/dHg(0) = −0.89 mol mol^{-1}, implying in situ conversion of Hg(0) to RGM. They also present comparisons to our GEOS-Chem model results for that site, showing for the model a similar anticorrelation ($r^2 = 0.80$) and slope (dRGM/dHg(0) = −0.73 mol mol^{-1}) as in the observations, although the model cannot reproduce the magnitude of the observed RGM events which reached a maximum of 600 pg m^{-3}.

8. Deposition of Mercury to the United States

[34] Wet deposition measurements of mercury are made in the United States at an increasing number of sites through the Mercury Deposition Network (MDN) [*National Atmospheric Deposition Program*, 2003]. Figure 9 compares simulated and observed mercury wet deposition fluxes for 2003–2004. The model predicts the magnitude of wet deposition within 10% nationally and shows good spatial correlation ($r^2 = 0.69$). Wet deposition fluxes of mercury are low in the west and north, and maximum in the southeast, in both the observations and the model. This maximum in the model reflects a combination of high OH concentrations (low latitudes) and frequent precipitation, and originates from the global pool of Hg(0) that is converted to Hg(II) and then deposited. Simulated precipitation is highest in the southeast and low in the west, consistent with measurements. The measurements also show high wet deposition fluxes in the industrial Midwest, reflecting deposition of locally emitted Hg(II) and Hg(P); the model greatly underestimates this feature (simulating only a 2 μg m^{-3} yr^{-1} enhancement for the region). In the model, deposition of emitted Hg(II) is mostly dry instead of wet; Hg(II) is assumed to be in water-soluble gaseous form and thus has a high dry deposition velocity. Most of the wet deposition of locally emitted mercury in the model is from Hg(P), which accounts for only a small fraction of emitted reactive mercury (Figure 1) but has a low dry deposition velocity. The model wet deposition flux from regional sources could be much greater if Hg(II) were partitioned into the aerosol

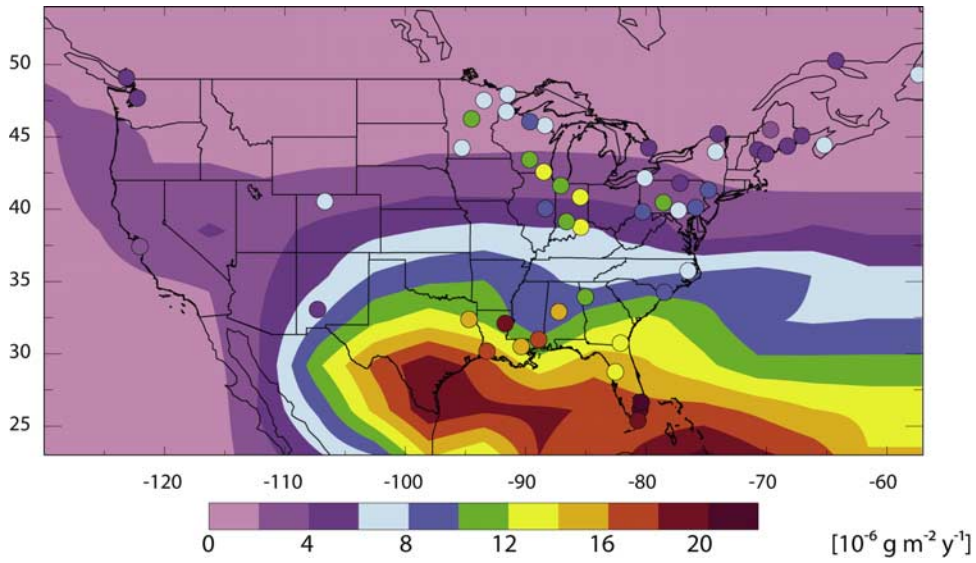

Figure 9. Annual mercury wet deposition fluxes over the United States for 2003–2004. Observations from the Mercury Deposition Network (circles) are compared to model results (background).

and thus less available for dry deposition. Better understanding of the gas-aerosol partitioning of Hg(II) is clearly needed. However, the total (wet plus dry) deposition flux from regional sources should be little affected.

[35] Figure 10 shows the percentage contribution from North American primary anthropogenic sources (not including reemission) to the total (wet plus dry) simulated mercury deposition in the United States, as determined from a sensitivity simulation with these sources shut off in the geographical domain covered by the Figure. The total simulated deposition flux over the United States is 152 Mg yr^{-1}, including 103 from dry and 49 from wet. The North American anthropogenic contribution to total mercury deposition averages 20% on a national basis but exceeds 50% in the industrial Midwest. Our results are consistent with the previous global model study by *Seigneur et al.* [2004], which found that North American anthropogenic emissions (including the United States, southern Canada and northern Mexico) contributed on average 30% to total deposition in the U.S., also with the highest contributions (up to 81%) in the Midwest. *Seigneur et al.* apportioned reemissions proportionally based on the region's contribution to overall anthropogenic emissions, which would increase the North American proportion.

9. Conclusions

[36] We have used a global 3-D atmospheric model (GEOS-Chem) coupled with an ocean model [*Strode et*

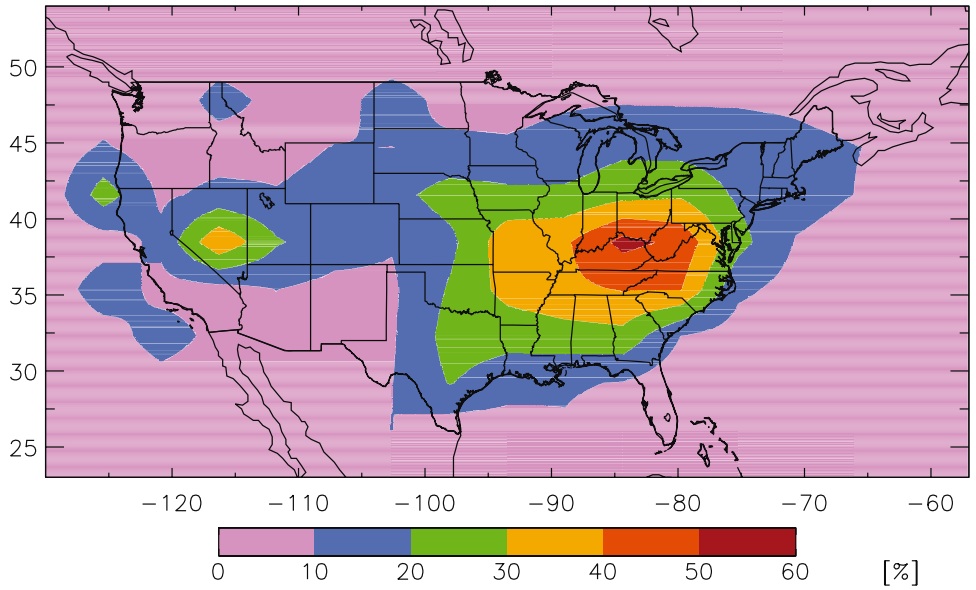

Figure 10. Percentage contributions from North American primary anthropogenic sources to total (wet plus dry) annual mercury deposition simulated in the model for 2003. North America is defined as the geographical domain shown in the figure.

al., 2006] to interpret the large ensemble of observations worldwide for total gaseous mercury (TGM) and reactive gaseous mercury (RGM) in terms of the constraints that they offer on the redox chemistry and deposition of atmospheric mercury. Given best estimates of mercury sources, we present here a plausible representation of the redox cycling and fate of atmospheric mercury that can account for some major features of the atmospheric observations. Evaluation of the model with oceanic observations is presented by *Strode et al.* [2006].

[37] Our model has a global mercury source of 7000 Mg yr^{-1}, including 2200 Mg yr^{-1} primary anthropogenic, 2000 Mg yr^{-1} from soils and terrestrial vegetation (of which 75% is reemission), and 2800 Mg yr^{-1} from the ocean (of which 87% is reemission). Oxidation of Hg(0) to Hg(II) is by OH (83%) and ozone, and removal of Hg(II) is by aqueous-phase photoreduction back to Hg(0) (55%), wet deposition (14%), dry deposition (21%), and uptake by sea-salt aerosols followed by deposition (10%). The resulting lifetime of total gaseous mercury (TGM) in the model is 0.79 years, at the low end of previous models (0.71–1.7 years).

[38] The model simulates without global bias the annual mean TGM concentrations observed at land-based sites, and accounts for 50% of the observed spatial variance at these sites. It greatly underestimates TGM observations from ship cruises in the northern hemisphere, which tend also to be higher than the land-based data for the corresponding latitudes. We have no satisfactory explanation for these high ship observations, which appear inconsistent with a dominant continental source for mercury as apparent for example from the Okinawa data of *Jaffe et al.* [2005]. The north-south interhemispheric ratio of surface air TGM concentrations in the model is at the low end of observed values, suggesting that the 0.8 years model lifetime for TGM is an upper limit given best estimates of emissions. However, the inconsistency between the land-based and ship data must be resolved for quantitative interpretation of the TGM interhemispheric ratio in terms of a TGM lifetime. Aircraft observations of the Hg(0) vertical profile up to 7 km show no systematic decrease with altitude, whereas the model has a slight decrease (10% over the depth of the troposphere). A TGM lifetime shorter than 0.8 years would seem inconsistent with the aircraft data.

[39] TGM observations at northern midlatitudes sites show on average a significant winter maximum and late summer minimum with 9% relative amplitude, and this is reproduced by the model. We show that a dominant OH sink for Hg(0) without compensating photoreduction would overestimate the seasonal amplitude, while a dominant ozone sink would not reproduce the seasonal phase. The observed seasonal variation of TGM is evidence for a photochemical sink of Hg(0). *Calvert and Lindberg* [2005] have argued that oxidation of Hg(0) to Hg(II) by OH, as implemented here using the laboratory data of [*Pal and Ariya*, 2004a; *Sommar et al.*, 2001], would not actually take place at a significant rate in the atmosphere due to decomposition of the HgOH adduct. *Holmes et al.* [2006] have recently proposed that oxidation by Br atoms in the middle and upper troposphere could provide a major global photochemical pathway for conversion of Hg(0) to Hg(II), based on the Hg-Br chemistry mechanism developed by *Goodsite et al.* [2004]. Testing this hypothesis will require better characterization of bromine radical chemistry in the troposphere as well as better quantification of Hg-Br kinetics and pathways.

[40] Global estimates of mercury sources are uncertain, and *Lindberg et al.* [2004] note that recent analyses of mercury emissions have estimated a number of additional sources (e.g., land emissions up to 3400 Mg yr^{-1}, increased biomass burning and volcanic emissions, Asian anthropogenic emissions). Increasing emissions in our model would require a decrease in the TGM lifetime in order to accommodate the observed TGM surface air concentrations. There is sufficient uncertainty in the redox chemistry of mercury, as discussed in section 2, that this could be achieved either by increasing the Hg(0) oxidation rate constants, decreasing the Hg(II) reduction rate constant, or including Br as an additional global oxidant for Hg(0) [*Holmes et al.*, 2006]. One would still need to reproduce the observed relative seasonal amplitude at northern midlatitude sites as a test of the chemistry (Figure 4), but the data are noisy and the different seasonal signatures expected from oxidation of Hg(0) by OH and ozone mean that one could still accommodate this constraint with a shorter TGM lifetime. The strongest objection against a large increase in global anthropogenic emissions comes in our view from the wet deposition flux data over the United States (section 8). We presently reproduce those data without national bias. A large increase in global mercury emissions would cause positive bias unless one were to invoke an increased role for dry deposition vs. wet. However, as discussed in section 8, there is evidence that the dry/wet deposition ratio is overestimated in the model.

[41] Observations of Hg(0), RGM, and CO at Okinawa by *Jaffe et al.* [2005] show a strong Hg(0)-CO correlation driven by Asian outflow, and this is reproduced by the model. The resulting dHg(0)/dCO enhancement ratio implies that the Asian source in the model (590 Mg yr^{-1} primary anthropogenic from the GEIA 2000 inventory, 340 Mg yr^{-1} land reemission, 120 Mg primary land emission) is 30% too low. RGM concentrations at Okinawa are not correlated with Hg(0) or CO, either in the model or in the observations, reflecting in the model a dominant source from subsidence. The observations show a large diurnal variation of RGM with peak at 13 LT and broad minimum at night. Reproducing this diurnal variation in the model requires a very fast sink, for which we invoke uptake by sea-salt aerosols with a lifetime of 7 hours. RGM observations in Florida offer some evidence of this uptake [*Guentzel et al.*, 2001]. Pacific cruise observations by *Laurier et al.* [2003] also show low RGM concentrations consistent with sea-salt aerosol uptake. Oxidation of Hg(0) by OH in the model can then explain the observed diurnal amplitude of RGM at Okinawa, but the daytime increase does not begin as early in the model as in the measurements, suggesting an additional pathway of Hg(0) oxidation by Br atoms [*Hedgecock et al.*, 2003].

[42] Oxidation of Hg(0) to RGM in the model occurs at all altitudes, while reduction is simulated as an in-cloud aqueous reaction that is mostly confined to the lower and middle troposphere. A consequence is that the RGM/TGM ratio increases with altitude, from 1–2% on average in surface air to 15–20% in the upper troposphere. RGM is the dominant form of mercury in the model stratosphere. The

simulated rise in RGM with altitude is consistent with the few aircraft and mountaintop measurements available. In particular, observations by *Swartzendruber et al.* [2006] at Mt. Bachelor (Oregon, 2.7 km altitude) show generally elevated levels of RGM with high episodes associated with downwelling air, and an anticorrelation between Hg(0) and RGM. *Swartzendruber et al.* [2006] show that our GEOS-Chem model results at Mt. Bachelor are qualitatively consistent with their observations although the model does not capture the magnitude of the RGM episodes. Recent observations in the lower stratosphere by *Murphy et al.* [2006] suggest that most of the mercury there is particulate bound and in the Hg(II) state.

[43] Observations from the Mercury Deposition Network (MDN) [*National Atmospheric Deposition Program*, 2003] in the United States show a maximum wet deposition flux in the southeast and a secondary maximum in the industrial Midwest. We reproduce the southeast maximum in GEOS-Chem and attribute it to photochemical oxidation of Hg(0) and frequent precipitation. The midwestern deposition enhancement in the model is much weaker than in the observations; it is mainly driven by regional emissions of refractory particulate mercury (Hg(P)), because emitted Hg(II) in the model is assumed to remain in the gas phase and is therefore preferentially removed by dry deposition. Better understanding of Hg(II) gas-aerosol partitioning is greatly needed. In the model, dry processes account for 68% of total mercury deposition in the United States, but the discrepancy with MDN observations in the Midwest suggests that this fraction is too high, possibly because Hg(II) should be partitioned into the particulate phase. We find in our model that 20% of total mercury deposition in the United States results from North American anthropogenic sources.

[44] **Acknowledgments.** This work was funded by the Atmospheric Chemistry Program of the U.S. National Science Foundation, by a U.S. Environmental Protection Agency (EPA) Science to Achieve Results (STAR) Graduate Fellowship to NES, and by the EPA Intercontinental Transport of Air Pollutants (ICAP) program. EPA has not officially endorsed this publication and the views expressed herein may not reflect the views of the EPA.

References

Alexander, B., R. J. Park, D. J. Jacob, Q. B. Li, R. M. Yantosca, J. Savarino, C. C. W. Lee, and M. H. Thiemens (2005), Sulfate formation in sea-salt aerosols: Constraints from oxygen isotopes, *J. Geophys. Res.*, *110*, D10307, doi:10.1029/2004JD005659.

Baker, P. G. L., E. G. Brunke, F. Slemr, and A. M. Crouch (2002), Atmospheric mercury measurements at Cape Point, South Africa, *Atmos. Environ.*, *36*, 2459–2465.

Banic, C. M., S. T. Beauchamp, R. J. Tordon, W. H. Schroeder, A. Steffen, K. A. Anlauf, and H. K. T. Wong (2003), Vertical distribution of gaseous elemental mercury in Canada, *J. Geophys. Res.*, *108*(D9), 4264, doi:10.1029/2002JD002116.

Bergan, T., and H. Rodhe (2001), Oxidation of elemental mercury in the atmosphere: Constraints imposed by global scale modelling, *J. Atmos. Chem.*, *40*, 191–212.

Bergan, T., L. Gallardo, and H. Rodhe (1999), Mercury in the global troposphere: A three-dimensional model study, *Atmos. Environ.*, *33*, 1575–1585.

Bey, I., D. J. Jacob, R. M. Yantosca, J. A. Logan, B. D. Field, A. M. Fiore, Q. B. Li, H. G. Y. Liu, L. J. Mickley, and M. G. Schultz (2001), Global modeling of tropospheric chemistry with assimilated meteorology: Model description and evaluation, *J. Geophys. Res.*, *106*, 23,073–23,095.

Calvert, J. G., and S. E. Lindberg (2005), Mechanisms of mercury removal by O_3 and OH in the atmosphere, *Atmos. Environ.*, *39*, 3355–3367.

Ebinghaus, R., H. H. Kock, C. Temme, J. W. Einax, A. G. Lowe, A. Richter, J. P. Burrows, and W. H. Schroeder (2002), Antarctic springtime depletion of atmospheric mercury, *Environ. Sci. Technol.*, *36*, 1238–1244.

Edgerton, E. S., and J. J. Jansen (2004), Elemental Hg measurements in Atlanta, GA, USA: Evidence for mobile sources?, paper presented at 7th International Conference on Mercury as a Global Pollutant, RMZ-Mater. and Geoenviron., Ljubljana, Slovenia.

Frank, D. G. (1999), Mineral Resource Data System (MRDS) data in Arc-View Shape File Format, for Spatial Data Delivery Project, http://webgis.wr.usgs.gov/globalgis/metadata_qr/metadata%5Core_deposits.htm, U.S. Geol. Surv., Spokane, Wash.

Friedli, H. R., L. F. Radke, and J. Y. Lu (2001), Mercury in smoke from biomass fires, *Geophys. Res. Lett.*, *28*, 3223–3226.

Friedli, H. R., L. F. Radke, R. Prescott, P. Li, J.-H. Woo, and G. R. Carmichael (2004), Mercury in the atmosphere around Japan, Korea, and China as observed during the 2001 ACE-Asia field campaign: Measurements, distributions, sources, and implications, *J. Geophys. Res.*, *109*, D19S25, doi:10.1029/2003JD004244.

Gårdfeldt, K., and M. Jonsson (2003), Is bimolecular reduction of Hg(II) complexes possible in aqueous systems of environmental importance, *J. Phys. Chem. A*, *107*, 4478–4482.

Goodsite, M. E., J. M. C. Plane, and H. Skov (2004), A theoretical study of the oxidation of Hg^0 to $HgBr_2$ in the troposphere, *Environ. Sci. Technol.*, *38*, 1772–1776.

Guentzel, J. L., W. M. Landing, G. A. Gill, and C. D. Pollman (2001), Processes influencing rainfall deposition of mercury in Florida, *Environ. Sci. Technol.*, *35*, 863–873.

Gustin, M. S., G. E. Taylor Jr., and R. A. Maxey (1997), Effect of temperature and air movement on the flux of elemental mercury from substrate to the atmosphere, *J. Geophys. Res.*, *102*, 3891–3898.

Hall, B. (1995), The gas phase oxidation of elemental mercury by ozone, *Water Air Soil Pollut.*, *80*, 301–315.

Han, Y.-J., T. M. Holsen, P. K. Hopke, and S.-M. Yi (2005), Comparison between back-trajectory based modeling and Lagrangian backward dispersion modeling for locating sources of reactive gaseous mercury, *Environ. Sci. Technol.*, *39*, 1715–1723.

Heald, C. L., et al. (2003), Asian outflow and trans-Pacific transport of carbon monoxide and ozone pollution: An integrated satellite, aircraft, and model perspective, *J. Geophys. Res.*, *108*(D24), 4804, doi:10.1029/2003JD003507.

Hedgecock, I. M., and N. Pirrone (2004), Chasing quicksilver: Modeling the atmospheric lifetime of $Hg^0_{(g)}$ in the marine boundary layer at various latitudes, *Environ. Sci. Technol.*, *38*, 69–76.

Hedgecock, I. M., N. Pirrone, F. Sprovieri, and E. Pesenti (2003), Reactive gaseous mercury in the marine boundary layer: Modelling and experimental evidence of its formation in the Mediterranean region, *Atmos. Environ.*, *37*, S41–S49.

Holmes, C. D., D. J. Jacob, and X. Yang (2006), Global lifetime of elemental mercury against oxidation by atomic bromine in the free troposphere, *Geophys. Res. Lett.*, *33*, L20808, doi:10.1029/2006GL027176.

Jaffe, D., E. Prestbo, P. Swartzendruber, P. Weiss-Penzias, S. Kato, A. Takami, S. Hatakeyama, and Y. Kajii (2005), Export of atmospheric mercury from Asia, *Atmos. Environ.*, *39*, 3029–3038.

Kellerhals, M., et al. (2003), Temporal and spatial variability of total gaseous mercury in Canada: Results from the Canadian Atmospheric Mercury Measurement Network (CAMNet), *Atmos. Environ.*, *37*, 1003–1011.

Lamborg, C. H., K. R. Rolfhus, W. F. Fitzgerald, and G. Kim (1999), The atmospheric cycling and air-sea exchange of mercury species in the South and equatorial Atlantic Ocean, *Deep Sea Res., Part II*, *46*, 957–977.

Lamborg, C. H., W. F. Fitzgerald, J. O'Donnell, and T. Torgersen (2002), A non-steady-state compartmental model of global-scale mercury biogeochemistry with interhemispheric gradients, *Geochim. Cosmochim. Acta*, *66*, 1105–1118.

Landis, M. S., R. K. Stevens, F. Schaedlich, and E. M. Prestbo (2002), Development and characterization of an annular denuder methodology for the measurement of divalent inorganic reactive gaseous mercury in ambient air, *Environ. Sci. Technol.*, *36*, 3000–3009.

Laurier, F. J. G., R. P. Mason, L. Whalin, and S. Kato (2003), Reactive gaseous mercury formation in the North Pacific Ocean's marine boundary layer: A potential role of halogen chemistry, *J. Geophys. Res.*, *108*(D17), 4529, doi:10.1029/2003JD003625.

Lin, C.-J., and S. O. Pehkonen (1998), Two-phase model of mercury chemistry in the atmosphere, *Atmos. Environ.*, *32*, 2543–2558.

Lin, C.-J., and S. O. Pehkonen (1999), The chemistry of atmospheric mercury: A review, *Atmos. Environ.*, *33*, 2067–2079.

Lin, C.-J., P. Pongprueksa, S. E. Lindberg, S. O. Pehkonen, D. Byun, and C. Jang (2006), Scientific uncertainties in atmospheric mercury models: I. Model science evaluation, *Atmos. Environ.*, *40*, 2911–2928.

Lindberg, S. E., and W. J. Stratton (1998), Atmospheric mercury speciation: Concentrations and behavior of reactive gaseous mercury in ambient air, *Environ. Sci. Technol.*, *32*, 49–57.

Lindberg, S. E., P. J. Hanson, T. P. Meyers, and K.-H. Kim (1998), Air/surface exchange of mercury vapor over forests—The need for a reassessment of continental biogenic emissions, *Atmos. Environ.*, *32*, 895–908.

Lindberg, S., D. Porcella, E. Prestbo, H. Friedlie, and L. Radke (2004), The problem with mercury: Too many sources, not enough sinks, paper presented at 7th International Conference on Mercury as a Global Pollutant, RMZ-Mater. and Geoenviron., Ljubljana, Slovenia.

Lindqvist, O. (1991), Mercury in the Swedish environment—Recent research on causes, consequences and corrective methods, *Water Air Soil Pollut.*, *55*, xi–261, doi:10.1007/BF00542429.

Liu, H., D. J. Jacob, I. Bey, and R. M. Yantosca (2001), Constraints from ^{210}Pb and ^{7}Be on wet deposition and transport in a global three-dimensional chemical tracer model driven by assimilated meteorological fields, *J. Geophys. Res.*, *106*, 12,109–12,128.

Lynam, M. M., and G. J. Keeler (2006), Source-receptor relationships for atmospheric mercury in urban Detroit, Michigan, *Atmos. Environ.*, *40*, 3144–3155.

Malcolm, E. G., G. J. Keeler, and M. S. Landis (2003), The effects of the coastal environment on the atmospheric mercury cycle, *J. Geophys. Res.*, *108*(D12), 4357, doi:10.1029/2002JD003084.

Mason, R. P., and G.-R. Sheu (2002), Role of the ocean in the global mercury cycle, *Global Biogeochem. Cycles*, *16*(4), 1093, doi:10.1029/2001GB001440.

Mason, R. P., W. F. Fitzgerald, and F. M. M. Morel (1994), The biogeochemical cycling of elemental mercury—Anthropogenic influences, *Geochim. Cosmochim. Acta*, *58*, 3191–3198.

Munthe, J., et al. (2003), Distribution of atmospheric mercury species in northern Europe: Final result from the MOE project, *Atmos. Environ.*, *37*, S9–S20.

Murphy, D. M., P. K. Hudson, D. S. Thomson, P. J. Sheridan, and J. C. Wilson (2006), Observations of mercury-containing aerosols, *Environ. Sci. Technol.*, *40*(10), 3163–3167.

National Atmospheric Deposition Program (2003), Mercury Deposition Network (MDN): A NADP Network, http://nadp.sws.uiuc.edu/mdn/, NADP Program Office, Ill. State Water Surv., Champaign.

Nriagu, J. O. (1994), Mechanistic steps in the photoreduction of mercury in natural waters, *Sci. Total Environ.*, *154*, 1–8.

Nriagu, J., and C. Becker (2003), Volcanic emissions of mercury to the atmosphere: Global and regional inventories, *Sci. Total Environ.*, *304*, 3–12.

Pacyna, E. G., J. M. Pacyna, F. Steenhuisen, and S. Wilson (2005), Global anthropogenic mercury emission inventory for 2000, *Atmos. Environ.*, *40*(22), 4048–4063.

Pal, B., and P. A. Ariya (2004a), Gas-phase HO-initiated reactions of elemental mercury: Kinetics and product studies, and atmospheric implications, *Environ. Sci. Technol.*, *38*, 5555–5566.

Pal, B., and P. A. Ariya (2004b), Studies of ozone initiated reactions of gaseous mercury: Kinetics, product studies, and atmospheric implications, *Phys. Chem. Chem. Phys.*, *6*, 572–579.

Park, R. J., D. J. Jacob, B. D. Field, R. M. Yantosca, and M. Chin (2004), Natural and transboundary pollution influences on sulfate-nitrate-ammonium aerosols in the United States: Implications for policy, *J. Geophys. Res.*, *109*, D15204, doi:10.1029/2003JD004473.

Pehkonen, S. O., and C. J. Lin (1998), Aqueous photochemistry of mercury with organic acids, *J. Air Waste Manage. Assoc.*, *48*, 144–150.

Pleijel, K., and J. Munthe (1995), Modeling the atmospheric mercury cycle—Chemistry in fog droplets, *Atmos. Environ.*, *29*, 1441–1457.

Poissant, L., M. Pilote, P. Constant, C. Beauvais, H. H. Zhang, and X. H. Xu (2004a), Mercury gas exchanges over selected bare soil and flooded sites in the bay St. Francois wetlands (Quebec, Canada), *Atmos. Environ.*, *38*, 4205–4214.

Poissant, L., M. Pilote, X. Xu, H. Zhang, and C. Beauvais (2004b), Atmospheric mercury speciation and deposition in the Bay St. François wetlands, *J. Geophys. Res.*, *109*, D11301, doi:10.1029/2003JD004364.

Poissant, L., M. Pilote, C. Beauvais, P. Constant, and H. H. Zhang (2005), A year of continuous measurements of three atmospheric mercury species (GEM, RGM and Hg-p) in southern Quebec, Canada, *Atmos. Environ.*, *39*, 1275–1287.

Pyle, D. M., and T. A. Mather (2003), The importance of volcanic emissions for the global atmospheric mercury cycle, *Atmos. Environ.*, *37*, 5115–5124.

Renner, R. (2004), Rethinking atmospheric mercury, *Environ. Sci. Technol.*, *38*, 448A–449A.

Ryaboshapko, A., R. Bullock, R. Ebinghaus, I. Ilyin, K. Lohman, J. Munthe, G. Petersen, C. Seigneur, and I. Wangberg (2002), Comparison of mercury chemistry models, *Atmos. Environ.*, *36*, 3881–3898.

Schlüter, K. (2000), Review: Evaporation of mercury from soils. An integration and synthesis of current knowledge, *Environ. Geol.*, *39*, 249–271.

Schroeder, W. H., and J. Munthe (1998), Atmospheric mercury—An overview, *Atmos. Environ.*, *32*, 809–822.

Schroeder, W. H., K. G. Anlauf, L. A. Barrie, J. Y. Lu, A. Steffen, D. R. Schneeberger, and T. Berg (1998), Arctic springtime depletion of mercury, *Nature*, *394*, 331–332.

Seigneur, C., K. Vijayaraghavan, K. Lohman, P. Karamchandani, and C. Scott (2004), Global source attribution for mercury deposition in the United States, *Environ. Sci. Technol.*, *38*, 555–569.

Seigneur, S., P. Karamchandani, K. Lohman, and K. Vijayaraghavan (2001), Multiscale modeling of the atmospheric fate and transport of mercury, *J. Geophys. Res.*, *106*, 27,795–27,809.

Shia, R.-L., C. Seigneur, P. Pai, M. Ko, and N. D. Sze (1999), Global simulation of atmospheric mercury concentrations and deposition fluxes, *J. Geophys. Res.*, *104*, 23,747–23,760.

Sillman, S., F. Marsik, K. I. Al-Wali, G. J. Keeler, and M. S. Landis (2005), Models for the formation and transport of reactive mercury: Results for Florida, the northeastern U.S. and the Atlantic Ocean, paper presented at Fifth Air Quality Conference: Mercury, Trace Elements, SO_3 and Particulate Matter, Energy and Environ. Res. Cent., Arlington, Va.

Somerville, R. C. J., and L. A. Remer (1984), Cloud optical thickness feedbacks in the CO_2 climate problem, *J. Geophys. Res.*, *89*, 9668–9672.

Sommar, J., K. Gårdfeldt, D. Strömberg, and X. Feng (2001), A kinetic study of the gas-phase reaction between the hydroxyl radical and atomic mercury, *Atmos. Environ.*, *35*, 3049–3054.

Steffen, A., W. Schroeder, R. Macdonald, L. Poissant, and A. Konoplev (2005), Mercury in the Arctic atmosphere: An analysis of eight years of measurements of GEM at Alert (Canada) and a comparison with observations at Amderma (Russia) and Kuujjuarapik (Canada), *Sci. Total Environ.*, *342*, 185–198.

Streets, D. G., J. Hao, Y. Wu, J. Jiang, M. Chan, H. Tian, and X. Feng (2005), Anthropogenic mercury emissions in China, *Atmos. Environ.*, *39*, 7789–7806.

Strode, S., L. Jaegle, N. E. Selin, D. J. Jacob, R. J. Park, R. M. Yantosca, R. P. Mason, and F. Slemr (2006), Air-sea exchange in the global mercury cycle, *Global Biogeochem. Cycles*, doi:10.1029/2006GB002766, in press.

Sundqvist, H., E. Berge, and J. E. Kristiansson (1989), Condensation and cloud parameterization studies with a mesoscale numerical weather prediction model, *Mon. Weather Rev.*, *117*, 1641–1657.

Swartzendruber, P., D. A. Jaffe, E. M. Prestbo, P. Weiss-Penzias, N. E. Selin, R. Park, D. J. Jacob, S. Strode, and L. Jaeglé (2006), Observations of reactive gaseous mercury in the free troposphere at the Mount Bachelor Observatory, *J. Geophys. Res.*, *111*, D24301, doi:10.1029/2006JD007415.

Temme, C., R. Ebinghaus, J. W. Einax, and W. H. Schroeder (2003a), Response to comment on "Measurements of atmospheric mercury species at a coastal site in the Antarctic and over the south Atlantic Ocean during polar summer," *Environ. Sci. Technol.*, *37*, 3241–3242.

Temme, C., F. Slemr, R. Ebinghaus, and J. W. Einax (2003b), Distribution of mercury over the Atlantic Ocean in 1996 and 1999–2001, *Atmos. Environ.*, *37*, 1889–1897.

Wang, Y., D. J. Jacob, and J. A. Logan (1998), Global simulation of tropospheric O_3–NO_x-hydrocarbon chemistry: 1. Model formulation, *J. Geophys. Res.*, *103*, 10,713–10,726.

Weiss-Penzias, P., D. A. Jaffe, A. McClintick, E. M. Prestbo, and M. S. Landis (2003), Gaseous elemental mercury in the marine boundary layer: Evidence for rapid removal in anthropogenic pollution, *Environ. Sci. Technol.*, *37*, 3755–3763.

Wesely, M. L. (1989), Parameterization of surface resistances to gaseous dry deposition in regional-scale numerical models, *Atmos. Environ.*, *23*, 1293–1304.

Wilson, S. J., F. Steenhuisen, J. M. Pacyna, and E. G. Pacyna (2005), Mapping the spatial distribution of global anthropogenic mercury atmospheric emission inventories, *Atmos. Environ.*, *40*(24), 4621–4632.

D. Jaffe, Interdisciplinary Arts and Sciences, University of Washington, Bothell, 18115 Campus Way NE, Bothell, WA 98011-8246, USA.

D. J. Jacob, R. J. Park, N. E. Selin, and R. M. Yantosca, Harvard University, 29 Oxford Street, Cambridge, MA 02138, USA. (eckley@fas.harvard.edu)

L. Jaeglé and S. Strode, Department of Atmospheric Sciences, University of Washington, Box 351640, Seattle, WA 98195-1640, USA.